Received: 23 August 2019 | Revised: 13 January 2020 | Accepted: 17 January 2020

DOI: 10.1002/aoc.5595

Check for updates

Applied Organometallic Chemistry WILEY

FULL PAPER

Palladium (II) complexes chelated by 1-substituted-4-pyridyl-*1H*-1,2,3-triazole ligands as catalyst precursors for selective ethylene dimerization

Mohammed Cassiem Joseph[1] | **Andrew John Swarts**[2] | **Selwyn Frank Mapolie**[1]

[1]DST-NRF Centre of Excellence in Catalysis (c*change), Department of Chemistry and Polymer Science, Stellenbosch University, Private Bag 1, Matieland, 7601Stellenbosch, South Africa

[2]Catalysis and Synthesis Research Group, Focus Area for Chemical Resource BeneficiationNorth-West University, 11 Hoffman Street, Potchefstroom, 2520, South Africa

Correspondence
Selwyn Frank Mapolie, DST-NRF Centre of Excellence in Catalysis (cchange), Department of Chemistry and Polymer Science, Stellenbosch University, Private Bag 1, Matieland,7601. Stellenbosch, South Africa.
Email: smapolie@sun.ac.za

Funding information
National Research Foundation South Africa, Grant/Award Number: CPRR160408161799

A series of neutral as well as cationic palladium methyl complexes bearing 1-substituted-4-pyridyl-*1H*-1,2,3-triazole ligands were prepared and fully characterized by a range of analytical techniques. Conventional and 2D NMR spectroscopy as well as single-crystal X-ray diffraction analysis unambiguously determined the molecular structure of the complexes. The neutral complexes activated by methylaluminoxane were found to be effective catalysts in the ethylene dimerization reaction. The catalyst performance of the *in-situ*-generated active species was compared with the discrete cationic complexes of the same ligand scaffold. Activities and selectivities for the two systems were remarkably similar, pointing to similarities in the nature of the active species. Both catalytic systems showed a strong correlation of activity and selectivity with the nature of the ligand scaffold. Highest activities were attained when electron-withdrawing groups were incorporated into the triazole ring, while increasing steric bulk in the *ortho*-position on the pyridyl ring of the ligand led to the almost exclusive dimerization of ethylene with selectivities up to 94% observed toward 1-butene.

KEYWORDS

1,2,3-triazole, ethylene oligomers, palladium (II) complexes, palladium–methyl complexes, selective ethylene dimerization

1 | INTRODUCTION

The development of late transition metal catalysts containing bidentate nitrogen donor ligands for ethylene oligo- and polymerization has seen a huge amount of research interest over the past two decades.[1–3] The seminal work of Brookhart and co-workers on the use of α-diimine ligands in the development of highly active olefin oligo−/polymerization catalysts opened up a new area of research (Figure 1a). Depending on the ligand architecture, it has been demonstrated that it is possible to produce high-molecular-weight polyethylene when the steric bulk of the *ortho*-substituent on the aryl ring was increased.[4] These *ortho*-substituents essentially block the axial coordination sites of the metal which, in turn, inhibits associative ligand exchange, hindering chain transfer and favoring polymerization to produce high-molecular-weight polymers. Conversely, decreasing the steric bulk of these ligands adjacent to the metal center leads to the oligomerization of olefins.[5,6] Subsequent to these initial reports, attention has shifted to the design of new ligands in an effort to find highly active and more selective catalyst systems for ethylene oligomerization.[1,7,8] For example, Ojwach and co-workers recently developed a series of hemi-labile (imino)pyridine palladium complexes (Figure 1b) as catalyst precursors for ethylene oligomerization.[9] Activation of these complexes with methylaluminoxane

 © 2020 John Wiley & Sons, Ltd.

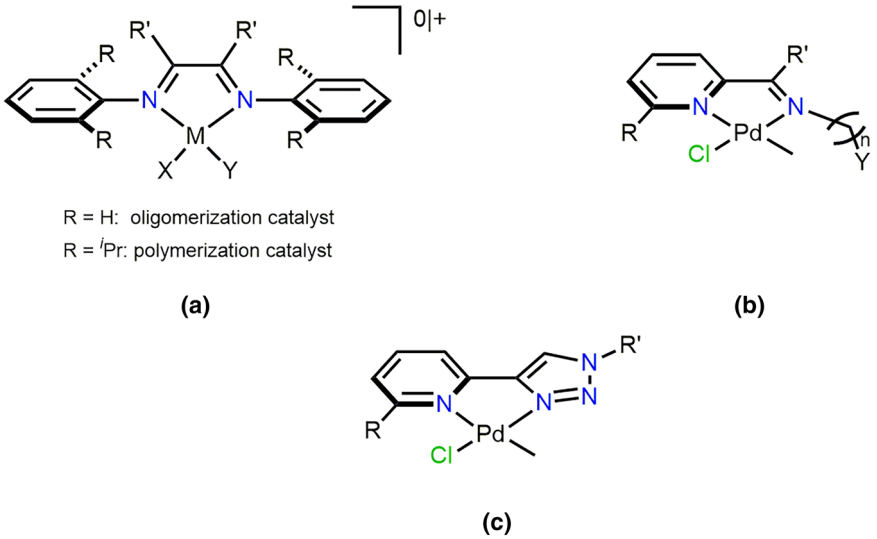

FIGURE 1 Oligo-/polymerization catalysts with different ligand settings: Brookhart's cationic α-diimine catalysts (a), Ojwach's hemilabile (imino)pyridine catalysts (b) and 1,2,3-triazole-pyridinato catalysts (c, this work)

(MAO) produced ethylene dimerization catalysts with high selectivity toward 1-butenes. Furthermore, these authors showed that catalytic activities could be controlled by varying the ligand architecture with the incorporation of different pendant arms onto the ligand backbone.

In an attempt to explore other N^N chelates as ligand scaffolds, we turned our attention to pyridyl-triazole ligands. This class of ligands have been gaining increasing significance owing to the fact that they can be regarded as functionalized analogs of the well-known 2,2′-bipyridine scaffold. The main advantage of the pyridyl-triazole ligands over the ubiquitous bipy type ligands is the ease of functionalization which can be obtained by using conventional Click chemistry. The ease of functionalization allows for facile fine-tuning of the electronic and steric properties of the ligand architecture. The Click-based synthetic approaches are less time-intensive than the synthetic methodologies required to functionalize bipy-based systems or even the conventional pyridine–imine ligand scaffolds. Herein we thus report on the synthesis and catalytic evaluation of a series of 1,2,3-triazole–pyridinato palladium complexes with different substituents on the pyridyl and triazole ring. The general structure of the system focussed on in this paper is illustrated in Figure 1c. Another feature of the complexes studied is the variation of the substituent in position 6 of the pyridyl unit of the ligand scaffold. We envisaged that variation of the type of the substituents in this position could perhaps impact on the regio-and chemoselectivity of the oligomerization process.

2 | RESULTS AND DISCUSSION

2.1 | Synthesis and characterization of 1-substituted-4-pyridyl-1*H*-1,2,3-triazole ligands, L1–L8

A series of alkyl- and aryl-substituted 1,2,3-triazolyl-pyridine ligands (**L1–L8**) were prepared by conventional and microwave-assisted copper-catalyzed alkyne-azide cycloaddition between the appropriate alkyl- or aryl azide (**A1–A5**) and 2-ethynylpyridine (**P2**, Scheme 1). In the case of ligands **L6** and **L7**, the starting alkynyl reagent was prepared via a Sonogashira coupling reaction between 2-bromo-6-methylpyridine and trimethylsilylacetylene followed by deprotection in the presence of KOH to afford 6-ethynyl-2-methylpyridine (**P3**). Incorporating a phenyl group onto the pyridyl ring firstly required a Suzuki-coupling between 2,6-dibromopyridine and phenylboronic acid, followed by a Sonogashira coupling and subsequent deprotection in the presence of KOH to afford 2-ethynyl-6-phenylpyridine (**P4**), which is the starting reagent for the preparation of ligand **L8** (Scheme 2). The low yield of **P4** is attributed to the formation of the by-product, 2,6-diphenylpyridine, which is observed in significant amounts during the Suzuki coupling. The ligands were isolated, after column chromatography, as air- and moisture-stable solids in moderate to excellent yields. The ligands varied in colour from yellow to dark red/brown. Several of the ligands except **L3** and **L6–L8** have been reported previously.[10–13] Ligands **L1–L8** were characterized by a variety of spectroscopic and analytical

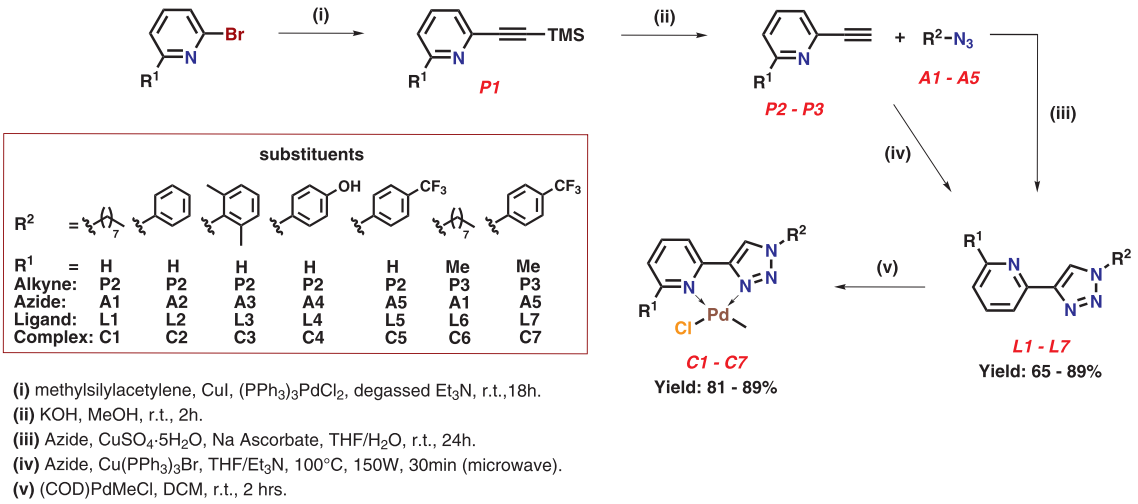

SCHEME 1 Synthesis of 1-substituted-4-pyridyl-*1H*-1,2,3-triazole ligands (**L1–L7**) and their palladium methyl complexes (**C1–C7**)

techniques. Briefly, Fourier transform-infrared (FT-IR) spectroscopy displayed the pyridyl ring ν(C=N) absorption band in the range 1593–1606 cm^{-1}. ^{1}H NMR spectra of the compounds revealed the triazole proton as a singlet and the imine proton of the pyridyl ring as a doublet in the range δ 8.56–9.49 ppm and δ 8.59–8.66 ppm respectively in DMSO-d_6. The bulk purities of ligands **L3** and **L6–L8** were confirmed by elemental analysis.

2.2 | Synthesis and characterization of 1,2,3-triazolyl-pyridinato-palladium methyl-chloride complexes, C1–C8

The reaction of ligands **L1–L8** with the methylpalladium (II) precursor, [(COD)PdMeCl], in dichloromethane (DCM) afforded the 1,2,3-triazolyl-pyridinato palladium (II)methyl-chloride complexes, **C1–C8**. The complexes were isolated as pale-yellow/off-white/amorphous solids in moderate to excellent yields of 56–89% (Schemes 1 and 2). Complexes **C2–C4** displayed solubility only in dimethyl sulfoxide. The solubility of the complexes improved significantly when the aryl substituent on the triazole moiety was replaced by an octyl chain. In fact, **C1** and **C6** are the only complexes that are soluble in chlorinated solvents. The solubility of the aryl-substituted complexes improved slightly when a trifluoromethyl substituent (complexes **C5**, **C7** and **C8**) was introduced onto the aryl ring. Characterization of these complexes by FT-IR spectroscopy revealed a shift to higher wavenumbers of the ν(C=N) absorption band of the pyridine unit which

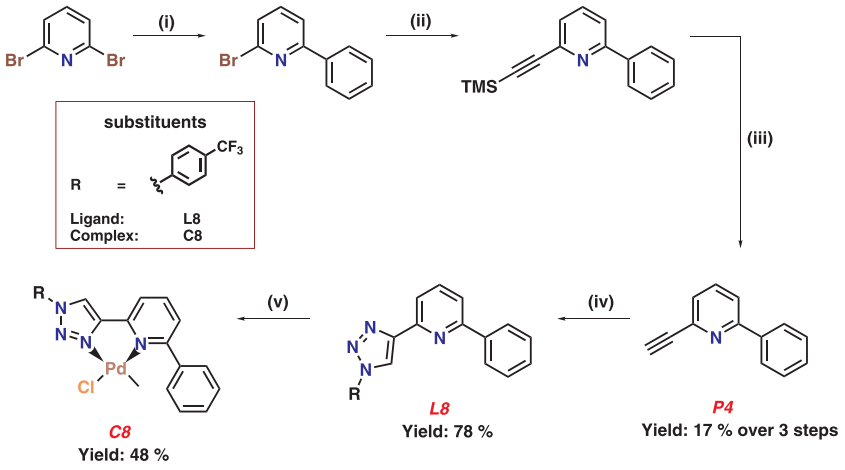

SCHEME 2 Synthesis of 1-substituted-4-phenylpyridyl-*1H*-1,2,3-triazole ligand (**L8**) and the palladium methyl complex (**C8**)

occurred in the range 1598–1615 cm^{-1}, confirming coordination to the metal.[14] The ^1H NMR spectra of the complexes (see Supporting Information) provided further evidence of ligand coordination to palladium. Specifically, the signal of the proton in position 6 of the pyridine ring was shifted downfield and observed in the range δ 8.68–8.79 ppm in DMSO-d_6. The electronic properties of these complexes are demonstrated by the relative chemical shift of the signal for triazole proton in the ^1H NMR spectrum of the complexes (Figure S71†). As the electron-donating ability of the substituent on the triazole ring increases, the signal for triazole proton becomes more shielded. This is due to the electron density within the triazole ring increasing. Further characterization by ESI–MS analysis revealed characteristic isotope clusters corresponding to $[M - Cl]^+$ and $[M - Cl + MeCN]^+$ fragments (see Supporting Information).[15,16] Lastly, elemental analysis confirmed the composition and bulk purity of the complexes.

Owing to the asymmetrical nature of the neutral complexes, the structural geometry of these complexes was probed in more detail. The complexes can adopt two possible isomers, i.e. isomer 1 (Figure 2a), in which the Pd–Me bond is *cis* relative to the pyridyl ring, and isomer 2 (Figure 2b), where the Pd–Me bond is *trans* relative to the pyridyl ring.

^1H NMR spectroscopy provides evidence for the formation of only one isomer in solution. ^1H NMR spectra of the all the complexes reveal only one isomer present in solution. To determine the relative position of the methyl ligand in the complexes, a 2D NOESY experiment was performed using complex **C1** in chloroform (Figure S39†). The spectrum shows no evidence for any interaction between the pyridyl-imine proton (H^1) and the protons of the methyl group, as evidenced by the absence of a cross-peak in the NOESY spectrum. This result suggests that isomer 2 in which the methyl is *trans* to the pyridine nitrogen is the one present in solution. In addition to relying on the NOESY experiment, we also employed an approach reported by Elsevier and co-workers[17] in which coordination induced chemical shifts were used to deduce the relative position of the proton in position 6 of the pyridyl ring relative to the Cl or methyl ligands. These authors showed that for various palladium methyl–chloride complexes, which contained pyridyl based N^N chelates, upfield coordination-induced shifts were indicative of the proton in position 6 of the pyridyl ring being in close proximity to the methyl ligand rather than the chloride. If the latter situation prevailed, one would have expected that chloride ligand with its relatively higher deshielding ability should show a strong downfield coordination-induced shift. This is indeed what we observed for our complexes, with the signal for the pyridyl proton in position 6, becoming deshielded on coordination to the palladium center. Thus, in conjunction with the 2D NOESY, we can conclude that in solution, the isomer in which the Cl ligand is *cis* to the pyridine nitrogen is the dominant species in solution. This is unlike the situation for the unsymmetrical α-diimine complexes reported by Guo *et al.*,[18,19] where mostly mixtures of both *cis* and *trans* isomers were detected. These authors found that, in cases where bulky substituents were incorporated into the ligand framework, the amount of the *cis* isomer present increases.

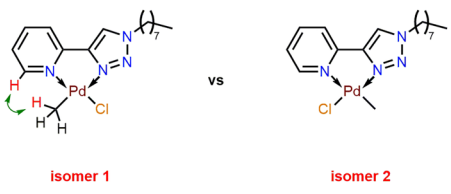

FIGURE 2 The two possible isomers for palladium complex **C1**: (a) isomer 1, Pd–Me bond *cis* relative to the pyridyl ring and (b) isomer 2, Pd–Me bond *trans* relative to the pyridyl ring

The molecular structures of complexes **C1**, **C4**, **C5** and **C7** were unambiguously determined by single-crystal X-ray diffraction analysis. The crystallographic data, which include selected bond lengths, bond angles and torsion angles, are presented in Tables S2† and S3†, respectively. The molecular structures of the complexes show coordination of the ligand through the pyridyl-N atom and the proximal-N atom of the triazole ring (Figure 3). For all complexes, the geometry around the palladium center corresponds to a slightly distorted square planar arrangement with the largest extent of distortion observed in the chelating N(1)–Pd(1)–N(2) bite angles. In general, the Pd–N(py) bond distances are longer than those involving the proximal-N atom of the triazole ring. For instance, the Pd–N(1) bond distance of complex **C1** [2.1785 (19) Å] is remarkably longer than Pd–N(2) owing to the *trans* influence exerted by the Pd–Me fragment. Similar trends were observed for other reported bidentate palladium methyl complexes.[20,21] The Pd–N(Py) bond length of the complexes is influenced by the substituent on the pyridyl-ring. Incorporating a methyl group adjacent to the pyridyl-N atom of the pyridine ring led to further elongation along the Pd–N(1) bond for complex **C7** (Figure 3). It is evident from these structures that the complexes adopt a geometry in which the chloride ligand is *cis* relative to the pyridyl nitrogen (isomer 2), correlating with the results obtained from 2D NOESY. Complex **C4** shows hydrogen bonding interaction between the solvate and the hydroxy moiety and in the case of **C5**, there is hydrogen bonding between the solvate and the triazole proton. **C7** shows no H-bonding between itself and any solvent molecules.

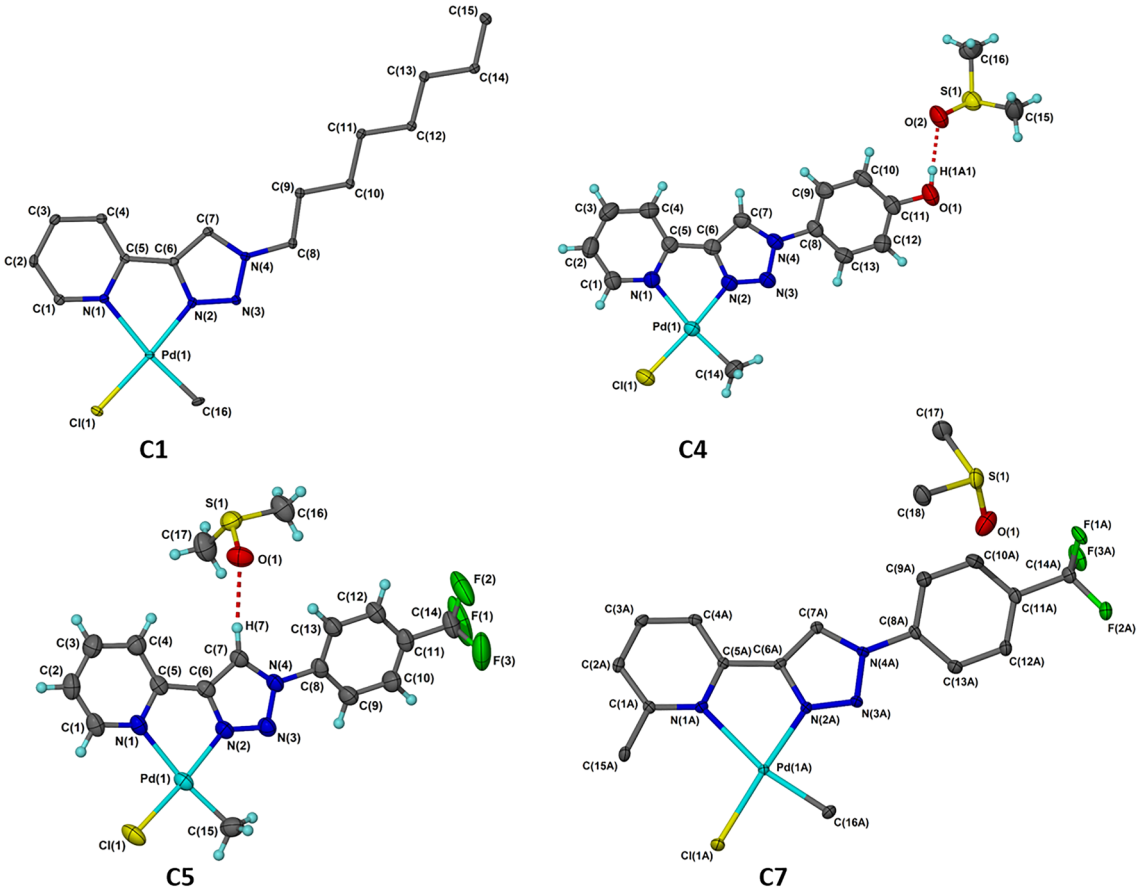

FIGURE 3 Molecular structure of complexes **C1**, **C4**, **C5** and **C7** with atomic numbering, drawn at 50% probability ellipsoids. The second independent structure (in the case of **C7**) and hydrogen atoms are omitted for clarity (in the case of **C1** and **C7**)

2.3 | Synthesis and characterization of cationic 1,2,3-triazolyl-pyridinato-palladium methyl complexes, C9–C11

Initially, during the application of complexes **C1–C8** in catalytic ethylene oligomerization, we generated the cationic active species *in-situ* using MAO as an activator. Subsequent to this, we attempted to prepare discrete single-site cationic complexes using $NaBAr^{F}{}_{4}$ as a chloride abstractor. This, unfortunately, led to the formation of unstable $BAr^{F}{}_{4}{}^{-}$ adducts when attempting to isolate the complexes as Et_2O and CH_3CN solvates. We then attempted to isolate the cationic species using pyridine as a solvent. Although the pyridine solvate appeared relatively more stable, the reaction unfortunately consistently yielded a mixture of the target cationic complex as well as a cationic by-product $[Pd(pyridine)_3CH_3]^+$ (Figure 4). The latter was always present in significantly large amounts. Figure S74† (Supporting Information) shows a ^1H NMR spectrum of the mixture containing the tris (pyridine)methyl palladium by-product. The formation of this species as a by-product has previously been detected

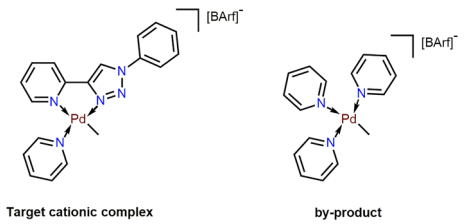

FIGURE 4 Target cationic palladium methyl complex (left) with the formation of the by-product, tris(pyridine)palladium methyl complex (right)

in the preparation of other cationic Pd–methyl complexes.[16]

Several attempts to vary the reaction conditions with the hope of enhancing the production of the target cationic species were fruitless. In addition, attempts to separate the target complexes from the $[Pd(pyridine)_3CH_3]^+$ by-product were also not successful. Thus, not being able to isolate the target $BAr^{F}{}_{4}{}^{-}$ adducts in pure form forced us to explore the use of an alternative anion as a counterion to the target cationic species. In this regard, we investigated the use of $PF_6{}^{-}$ as a counterion, and fortunately,

this gave stable cationic complexes that we were able to isolate in a pure form. The cationic complexes with PF_6^- as counterion, **C9–C11**, were prepared by the reaction of the corresponding neutral complexes (**C5**, **C7** and **C8**) with a chloride abstractor, $AgPF_6$, in the presence of acetonitrile as the weakly coordinating solvent (Scheme 3). These complexes were isolated in high yields (81–88%), and they displayed solubility in acetonitrile and DMSO and were partially soluble in chlorinated solvents. The cationic PF_6^- complexes were characterized by a range of analytical techniques. In the FT-IR spectra, the ν(CN) stretching frequency is shifted to slightly higher wavenumbers (in the range 1615–1618 cm^{-1}). Furthermore, the appearance of an upfield singlet in the range 1.50–1.75 ppm in the ^1H NMR spectra of the complexes can be assigned to the methyl protons of acetonitrile coordinated to the Pd center. The molecular structure of complex **C11** was also unambiguously determined by single-crystal X-ray diffraction analysis. Selected crystallographic data for this complex are tabulated in Tables S2† and S3† in the Supplementary Information. The molecular structure of **C11** shows a dissociated ion-pair in which the separation of the cation and anion is represented by a Pd–P distance of 5.625 Å. The coordination sphere of the metal is occupied by the chelating pyridyl-triazole and the methyl ligands. The fourth coordination site is occupied by a weakly coordinating acetonitrile molecule which occurs *cis* to the pyridyl nitrogen donor atom (Figure S72†). The geometry around the metal center corresponds to a distorted square planar arrangement, with the largest deviation observed in the N(1)–Pd(1)–N(5) angle (102.14°) as a result of acetonitrile coordination. For the cationic complex, the Pd–N(1) bond distance was also remarkably longer than Pd–N(2) owing to the *trans* influence of the methyl group. Interesting to note was the relative orientation of the phenyl substituent in the 6-position on the pyridyl ring. The torsion angle C(2)–C(1)–C(15)–C(16) is −48.1(2), which reveals that the phenyl substituent and pyridyl ring are perpendicular to each other, hence the phenyl group could induce some sort of steric control around the metal center.

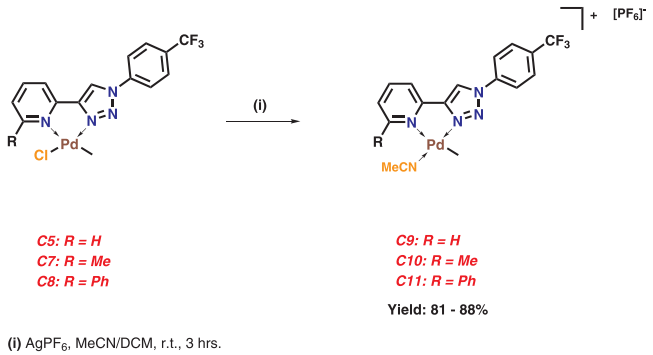

SCHEME 3 Synthesis of cationic 1,2,3-triazolyl-pyridinato-palladium methyl complexes, **C9–C11**

2.4 | Ethylene oligomerization reactions

Preparative-scale ethylene oligomerization was conducted at room temperature employing neutral complexes **C1–C8** as pre-catalyst in the presence of a co-catalyst, MAO (Scheme 4). In a typical experiment, 10 μmol of the complex was reacted with excess co-catalyst in toluene and stirred at various pressures, temperatures and reaction times.

2.4.1 | Ethylene oligomerization reactions employing neutral complexes C1–C8 as pre-catalyst

Complexes **C1–C8** were evaluated as pre-catalysts, and the results are summarized in Table 1. The complexes, upon activation with MAO, oligomerize ethylene with the highest turnover frequency (TOF) of 5594 obtained for complex **C5** (Table 1, entry 5). The product distribution consists mainly of C_4 products with small amounts of C_6 and C_8 oligomers observed. The higher selectivity toward C_4 products can be attributed to the absence of steric crowding around the metal center, a well-known factor in controlling the product distribution.[4,6] Brookhart and co-workers reported the application of cationic palladium phosphine-oxazoline complexes in ethylene oligomerization.[22] Complexes containing sterically bulky ligands in axial positions yielded a Schulz–Flory distribution of longer-chain α-olefins with the highest TOF value of 15760 h^{-1} obtained. In these examples reported by Brookhart, the ligands have sufficient steric bulk to effectively block chain transfer to a significant degree, thus leading to long-chain α-olefins. However, in the absence of axial steric bulk, only ethylene dimerization was observed. This is indeed what we also observe. It is therefore not surprising that in our case, complexes **C1–C5** show similar product distributions owing to their similar steric characteristics around the metal center. In addition, the major component of the C_4 fraction consists largely of 2-butene isomers with the larger fraction being *trans*-2-butene. This is largely due to the fact that the originally formed 1-butene can readily undergo isomerization under the reaction conditions employed. This is not surprising as Pd complexes with N^N chelating ligands systems are known to easily undergo facile isomerization, especially if ligands are not

SCHEME 4 Preparative-scale ethylene oligomerization employing neutral complexes

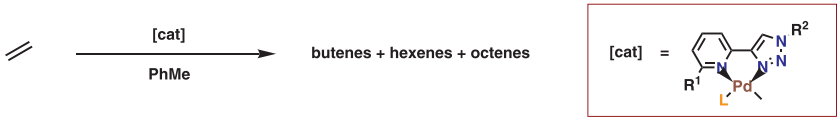

TABLE 1 Preparative-scale ethylene oligomerization employing complexes **C1**–**C8** as catalyst precursors[a]

			Product distribution and selectivity (%)[c]			
Entry	**Complex**	**TOF[b]**	**C_4**	**C_6**	**C_8**	**1-C_4:2-C_4[d]**
1	**C1**	2857	80	15	5	45: 55
2	**C2**	5118	82	13	5	43: 57
3	**C3**	4404	79	15	6	43: 57
4	**C4**	4483	81	13	6	44: 56
5	**C5**	5594	81	15	4	45: 55
6	**C6**	2222	89	7	4	73: 27
7	**C7**	4682	92	5	3	71: 29
8	**C8**	4205	93	6	1	94: 6

[a]Reaction conditions: catalyst loading, 10 μmol; pressure, 20 bar; temperature, 30°C; time, 1 h; co-catalyst, MAO; Al:Pd, 1000:1; solvent, PhMe (40 ml). [b] Turnover frequency (TOF) in units of $mol_{ethylene}$ mol Pd^{-1} h^{-1}. [c] Determined by GC-FID. [d] The ratio of *trans*- to *cis*-2-butenes is approximately 2:1 in most cases.

sterically demanding. In a recent paper by Albrecht and co-workers, they also observed extensive 1-butene isomerization while performing ethylene dimerization using pyridylidene-amide palladium complexes.[23]

Incorporating a methyl group in the *ortho*-position on the pyridyl ring led to a significant improvement in the selectivity toward 1-butene. For example, ethylene dimerization catalyzed by complexes **C6** and **C7** displayed a 26–28% increase in the amount of 1-butene produced under the same reaction conditions. However, for these catalysts lower activities were observed (Table 1, entries 6 and 7). Complex **C8** in which the bulkier phenyl group is incorporated into the ligand architecture displayed a significant increase in selectivity with 94% of the product mixture being 1-butene (Table 1, entry 8). It is evident from these results that the steric bulk imparted by the large phenyl group in the *ortho*-position slows down the re-coordination and subsequent isomerization of 1-butene to yield 2-butenes (Scheme 5). This is also supported by the observation that less trimerization and tetramerization products were produced by those catalysts possessing some degree of steric bulk in the position *ortho* to the pyridine nitrogen. The fact that no polymer or long-chain oligomer formation was observed indicates that the steric hindrance exerted by the phenyl group is not large enough to effectively block the axial positions of the metal center, which allows β-H elimination to still proceed in the presence of the phenyl group. In a similar study, Albrecht and co-workers developed a series of palladium carbene complexes which contain different C^N bidentate NHC–pyridine ligands with varying steric characteristics.[24] Selective dimerization of ethylene was observed in the presence of the bulky 2,6-dimethylphenyl substituent on the pyridyl-ring. However, when the steric strain is reduced, a mixture of low molecular weight oligomerization products is isolated.

In the case of our complexes, the nature of the substituent on the triazole ring, although not affecting regio-selectivity, had a marked effect on the activity of the complexes. Higher activities were achieved when aryl groups were incorporated as a substituent on the triazole ring. For instance, the TOF of the reaction increased significantly when the octyl substituent on the triazole ring was replaced with a phenyl group (Table 1, entry 1). Increasing the electron-withdrawing nature of the aryl ring by incorporating groups such CF_3 as substituents led to an increase in TOF from 5118 (**C2**) to 5594 (**C5**) (Table 1, entries 2 and 5). On the other hand, electron-donating groups on the aryl substituent led to a decrease in the catalytic activities with TOF's of 4404 and 4483 being achieved for complexes **C3** and **C4** respectively (Table 1, entries 2–4). The enhanced catalytic performance achieved with electron-withdrawing substituents is attributed to the fact that these substituents enhance the overall electrophilicity of the metal center, hence promoting monomer coordination. Jordan and co-workers reported a series of cationic palladium alkyl complexes ligated by bis (heterocycle)methane ligands.[25,26] They showed that ethylene insertion rates were enhanced when the electrophilicity of the metal is increased as a

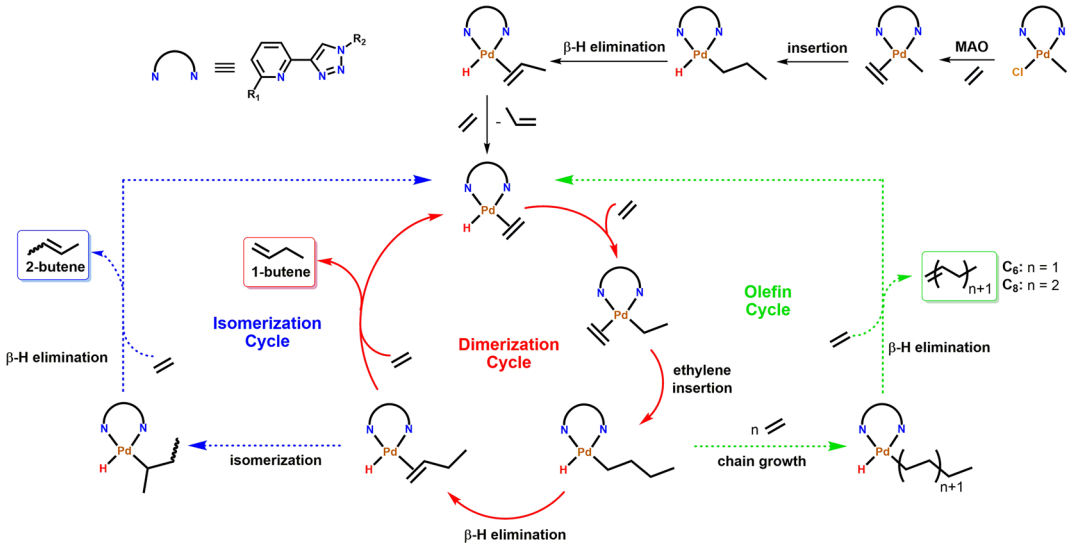

SCHEME 5 Proposed catalytic olefin dimerization, isomerization and oligomerization cycles for **C1–C8**

result of a decrease in the sigma donor ability of the ligand.

2.4.2 | Effect of reaction conditions on ethylene oligomerization employing complexes C1, C5 and C8

Since these complexes were found to be active catalysts in the oligomerization of ethylene, the catalytic behavior of complexes **C1**, **C5** and **C8** was studied in more detail to explore the impact of various reaction conditions (Table 2). Increasing the ethylene pressures from 5 to 30 bar led to a dramatic increase in activity with a concomitant increase in selectivity toward butenes being observed (Table 2, entries 1–8). For example, TOF's of 1071 and 6665 were obtained for **C5** at 5 and 30 bar respectively with a 24% selectivity improvement toward butenes at the higher pressure. This is more likely due to the higher monomer concentration at the elevated pressure, which favors ethylene coordination to the metal center, resulting in less tri- and tetra-merization being observed. Interesting to note was the decrease in the amount of internal butenes produced at higher pressures. For instance, the percentage of internal butenes observed decreased from 69 to 42% when the pressure was increased from 5 to 30 bar, respectively (Table 2, entries 1 and 8). At higher pressures, the probability of 1-butene coordinating to the metal was lower when compared to ethylene; hence the isomerization process was retarded. Similar observations were made by Smith and co-workers in which the catalytic behavior for a series of palladium complexes for ethylene oligomerization was examined.[27] They found that the 1-butene component within the butene fraction gradually increased with an increase in the ethylene pressure from 10 to 50 bar. Although **C8** was not the most active catalyst, the complex preferentially dimerized ethylene with conversions of 86–88% and selectivity of around 89% toward 1-butenes being observed at lower ethylene pressures (Table 2, entries 3 and 6). It is evident from these results that the reaction conditions had minimal effect on butene selectivity in the case of **C8** and that the bulky phenyl group incorporated on the pyridine ring was actually responsible for the complex being more selective. In this instance, the phenyl group imposed steric congestion around the vacant site, which in turn limited the re-coordination and isomerization of 1-butene to produce internal butenes. Similarly, the formation of longer-chain olefins was less favored using complex **C8** as catalyst (Scheme 5).

Next, we investigated the effect of MAO concentration on ethylene oligomerization by varying the co-catalyst to catalyst ratio (Al:Pd) from 50:1 to 3000:1. Both complexes **C5** and **C8** were catalytically inactive when an Al:Pd ratio of 50:1 was employed (Table 2, entries 10 and 11). Increasing the Al:Pd ratio from 500:1 to 1000:1 led to an improvement in the activity from 3095 to 5594 and from 2063 to 4205 for **C5** and **C8** respectively (Table 1, entries 5 and 8; Table 2, entries 12 and 13). Increasing the Al:Pd ratio to 3000:1, however, led to a significant loss in activity with TOF values of 2857 and 2460 being observed for complexes **C5** and **C8** respectively (Table 2, entries 14–15). These results highlight the importance of careful control over the co-catalyst concentration, as catalyst deactivation seems to occur at Al:Pd ratios in excess of 1000:1, which is possibly due to an increase in trimethylaluminum impurities in the catalytic reaction mixture.[28,29]

TABLE 2 Effect of reaction pressure and co-catalyst loading on ethylene oligomerization employing complexes **C1**, **C5** and **C8** as catalyst precursors[a]

				Product distribution and selectivity (%)[c]			
Entry	**Complex**	**Pressure (bar)**	**TOF[b]**	**C_4**	**C_6**	**C_8**	**1-C_4:2-C_4[d]**
1	**C1**	5	793	71	20	9	30: 70
2	**C5**	5	1071	70	21	9	31: 69
3	**C8**	5	913	86	10	4	87: 13
4	**C1**	10	1785	75	18	7	36: 64
5	**C5**	10	2936	74	20	6	35: 65
6	**C8**	10	2261	88	8	4	89: 11
7	**C1**	30	3571	95	5	0	55: 45
8	**C5**	30	6665	94	6	0	58: 42
9	**C8**	30	4523	95	5	0	94: 6
10 [e]	**C5**	20	–	–	–	–	–
11 [e]	**C8**	20	–	–	–	–	–
12 [f]	**C5**	20	3095	82	13	5	43: 57
13 [f]	**C8**	20	2063	90	8	2	91: 9
14 [g]	**C5**	20	2857	81	13	6	45: 55
15 [g]	**C8**	20	2460	91	7	2	92: 8

[a]Reaction conditions: catalyst loading, 10 μmol; temperature, 30°C; time, 1 h; co-catalyst, MAO; Al:Pd, 1000:1; solvent, PhMe (40 ml). [b] TOF in units of $mol_{ethylene}$ mol Pd^{-1} h^{-1}. [c] Determined by GC-FID. [d] The ratio of *trans*- to *cis*-2-butenes is approximately 2:1 in most cases. [e] Al:Pd = 50 (MAO used as co-catalyst). [f] Al:Pd = 500 (MAO used as co-catalyst). [g] Al:Pd = 3000 (MAO used as co-catalyst).

In order to examine the neutral complexes in terms of catalyst stability, a series of additional catalytic reactions were conducted at various reaction times. A two-stage reaction profile was observed (Figure 5a). Increasing the reaction time from 0.5 to 1 h led to an initial increase in the activity of the catalysts. However, extending the reaction time to 2 h and beyond showed a decrease in activity. For example, increasing the reaction time to 1 h led to an increase in TOF from 4444 to 5594 for complex **C5**; however, lower TOFs were attained at 2 and 4 h respectively. In the case of **C1** and **C8**, the catalysts became almost completely inactive after 4 h, at which TOFs of 436 and 952 were observed, respectively. It is clear from these results that the catalyst systems show high initial activity but then gradually deactivate after about 1 h. Therefore, we can conclude that the complexes are stable within the first hour of the reaction after which it undergoes some degree of catalyst decomposition.[9,30] This is evidenced by the observation of small amounts of Pd black in the reaction mixture. Extended reaction times had minimal influence on the chemo- and regioselectivity of the complexes. In the case of the sterically less demanding catalyst precursors, **C1** and **C5**, there was only a slight increase in octene formation over time (Figure 5b and d). In addition, a slight increase in internal butene isomers was observed (Figure 5c and e). Both of these observations are probably due to the fact that, over time, the 1-butene formed can re-coordinate and become involved in either isomerization or chain extension processes (Scheme 5). The subsequent chain growth and/or isomerization of the initially formed 1-butene product occurred to a lesser degree for **C8** (Figure 5f and g). The bulky ligand would be expected to hinder both these processes as it impacts negatively on 1-butene coordination, which is a prerequisite for both processes.

2.5 | Ethylene oligomerization employing discrete cationic complexes C9–C11

In addition to utilizing the neutral Pd–methyl-chloride complexes as catalyst precursors to generate the cationic active species *in-situ*, we also briefly evaluated the use of discrete cationic Pd–Me complexes as catalysts. Thus, cationic complexes **C9–C11** were employed in the catalytic ethylene oligomerization reaction. The results of this investigation are summarized in Table 3. These discrete cationic complexes exhibit appreciable catalyst activity with TOF values ranging from 4364 to 5554 with complex **C9** which has only a H-substituent in position 6 on the pyridine, showing the highest activity. **C11** with the bulky phenyl substituent has the lowest activity. In the case of the latter, initial coordination of the alkene substrate is hindered by the presence of the relatively

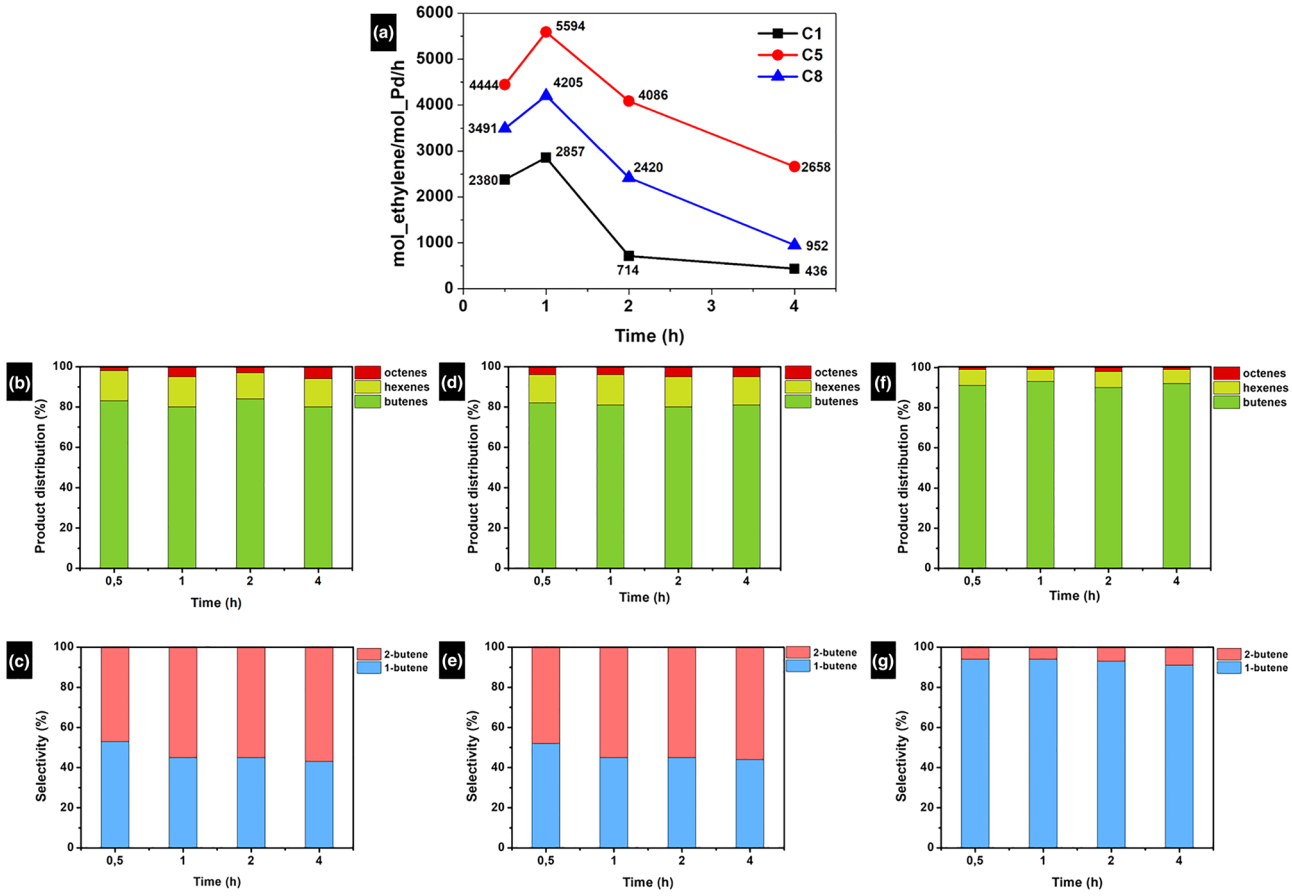

FIGURE 5 (a) Time profile for complexes **C1**, **C5** and **C8** showing significant loss in activity after 1 h. Product distribution and selectivity of (b and c) complex **C1**, (d and e) complex **C5** and (f and g) complex **C8** respectively over time

TABLE 3 Preparative-scale ethylene oligomerization employing cationic complexes **C9**–**C11** as catalyst precursors[a]

			Product distribution and selectivity (%) [c]			
Entry	**Complex**	**TOF[b]**	**C_4**	**C_6**	**C_8**	**1-C_4:2-C_4 [d]**
1	**C9**	5554	83	17	–	45: 55
2	**C10**	4761	90	10	–	74: 26
3	**C11**	4364	92	8	–	93: 7

[a]Reaction conditions: catalyst loading, 10 μmol; pressure, 20 bar; temperature, 30°C; time, 1 h; solvent, PhMe (40 ml). [b] TOF in units of $mol_{ethylene}$ mol Pd^{-1} h^{-1}. [c] Determined by GC-FID. [d] The ratio of *trans*- to *cis*-2-butenes is approximately 2:1 in most cases.

bulky phenyl group, slowing down the overall reaction rate. The trend with regards to the catalyst activity for the three discrete cationic complexes is similar to what was observed for the neutral analogs of these complexes (Table 1, entries 5–8). When comparing the activities of the neutral catalyst precursors activated by MAO at the optimum Al:Pd ratio of 1000:1 with those obtained using their discrete cationic analogs, we note a remarkable correlation between the two. This seems to indicate that the nature of the active species is similar in both cases. The discrete cationic complexes, however, outperform the MAO-activated neutral complexes when Al:Pd ratios either lower or higher than 1000:1 are employed. In terms of regio-selectivity, complex **C11** with the relatively bulky substituent in position 6 on the pyridine ring shows the highest production of 1-butene. A 1-butene:2-butene ratio of 93:7 is observed in this case (Table 3, entry 3). Once again, this is comparable with what was observed for the neutral analog, **C8** when activated with MAO using an Al:Pd ratio of 1000:1. These results seem to indicate in the case of the neutral complex that an optimum concentration of the cationic active species is generated *in-situ* at an Al:Pd ratio of 1000:1. Furthermore, the fact that similar catalytic activity

performance is observed for both the MAO-activated complexes and the discrete cationic complexes, seems to indicate a fair degree of similarity in the active species for the two types of systems employed. This is not unexpected since it is reasonably envisaged that the active species generated from both **C8** and **C11** would have similar ligand arrangements around the palladium center. The only difference we would expect between the two cationic intermediates would be the relative positions of the counterions since there is a considerable difference in the size of the two counterions. It would, however, appear that the latter does not significantly impact the oligomerization ability of the two catalytic systems as similar activities and selectivities are observed. Given the similarity in the catalytic behavior observed using both the neutral and the cationic catalyst precursors, it is also not unreasonable to conclude that a similar mechanistic pathway is operative for the two systems.

From the above discussion, it emerges that the reactivity of these palladium triazole pyridine complexes can be fine-tuned by careful selection of substituents on both the pyridine and triazole rings. The location of the substituents in these bifunctional ligand systems seems to be an important factor to consider when designing catalysts with the ligand system investigated in this study.

Thus, from the preliminary results, it would appear that substituents on the triazole ring component of the ligand scaffold have a greater influence on the activity of the catalyst system, while substituents in the pyridine ring, especially those in position 6, have a significant impact on the regioselectivity of the dimerization process. The latter, however also influences activity, but this is not as significant as its steric impact. These results reported here give some useful insight into catalyst design methodologies that could be adopted to improve selectivity in these triazole pyridine systems. This is currently forming the basis of ongoing research in our laboratory, where ligands such as those reported here are being designed for other catalytic applications.

3 | CONCLUSION

A series of neutral methyl-chloride–palladium complexes containing pyridine–triazole ligands as well as a series of cationic analogs in chloride displaced by acetonitrile were successfully employed as catalysts in ethylene oligomerization. The neutral complexes **C1–C5** activated with methylaluminoxane produced mainly butenes, with small quantities of hexenes and octenes also detected. Comparable catalytic results were obtained when the discrete cationic complexes **C9–C11** were employed as catalysts, pointing to similarities in the nature of the active species for both classes of complexes.

The catalyst activity of the complexes was essentially dictated by the nature of the substituent on the triazole component of the bifunctional ligand system. Electron-withdrawing substituents such as CF_3 enhance the electrophilicity of the metal center, which promotes the initial coordination of the alkene, resulting in higher activities.

Substituents in position 6 of the pyridine ring of the ligand scaffold on the other hand influence the selectivity of the catalysts. Ethylene dimerization was favored when the sterically bulky phenyl group was incorporated in the 6-position on the pyridyl ring, as was the case for complexes **C8** and **C11**. For these complexes, a regioselectivity approaching 95% toward 1-butene was observed. The results obtained demonstrate that both catalyst activity and selectivity are sensitive to ligand architecture and that both steric and electronic characteristics play a role in this regard. In the systems investigated here, these effects are however largely imparted by different components of the pyridine–triazole ligand scaffold. The initial results reported here provide valuable insights into the design of other potential alkene oligomerization catalysts based on these pyridine–triazole ligand scaffolds in which the constituent components control different aspects of the catalyst's performance.

4 | EXPERIMENTAL

4.1 | General

Unless otherwise stated, all reagents were acquired from Sigma-Aldrich, Merck and Alfa-Aesar and used without further purification. Solvents were obtained from Merck and Kimix and purified using Pure Solv™ micro solvent purifiers fitted with activated alumina columns. Selected ligands were purified by flash chromatography using an automated Isolera One Biotage flash chromatography unit, equipped with a 200–450 nm variable UV detector. Melting point determinations were recorded on a Stuart Scientific SMP3 apparatus and are reported as uncorrected. FT-IR analyses were performed on a Thermo Nicolet AVATAR 330 instrument with a smart ATR and recorded as neat samples. ^{1}H, ^{13}C and ^{31}P NMR spectra were recorded on Varian VNMRS 300 MHz and Varian Unity Inova 400 MHz spectrometers. The chemical shifts for proton and carbon spectra are referenced internally to the residual deuterated solvents and referenced externally to tetramethyl silane. Chemical shifts for ^{31}P NMR spectra are referenced externally

relative to 85% phosphoric acid (H_3PO_4). Elemental analyses were performed on a Vario EL cube elemental analyzer instrument. ESI–MS analyses were recorded on Waters API Quattro Micro and Waters API Q-TOF Ultima instruments by direct injections. The precursor [(COD)PdMeCl][17,31] and the aliphatic[32] and aromatic azides[33] were prepared according to literature procedures.

4.2 | NMR abbreviations

s = Singlet, d = doublet, t = triplet, dd = doublet of doublets, td = triplet of doublets, dt = doublet of triplets, dq = doublet of quartets, quin. = quintet, sept. = septet, m = multiplet (denotes complex pattern for a single proton resonance), comp. = complex (denotes complex pattern of overlapping proton resonances). Superscripts denote protons as per numbering scheme in Figure S1† in the Supporting Information document.

4.3 | Synthesis of ligands and complexes

The procedure for the preparation of ligand **L3**, neutral complex **C1** and cationic complex **C9** is given below as representative examples. Detailed characterization data of all other ligands and complexes prepared are discussed in the Supporting Information†.

4.3.1 | Synthesis of 1-(2,6-dimethylphenyl)-4-pyridyl-*1H*-1,2,3-triazole ligand (L3)

This method was adopted and modified according to a literature procedure.[34] To a 10 ml microwave tube was added Cu $(PPh_3)_3Br$ (0.02 g, 0.02 mmol) followed by Et_3N (2 ml), 2-ethynylpyridine (0.38 ml, 3.8 mmol), 2-azido-1,3-dimethylbenzene (0.62 g, 4.2 mmol) and dry THF (2 ml) after which the tube was sealed and placed in the microwave reactor (time, 30 min, temperature, 100 °C and power, 150 W). After the allotted time, the reaction mixture was allowed to cool to room temperature and the solvent removed *in vacuo* to afford a dark-brown residue. H_2O (40 ml) was added, and the product was extracted with DCM (3 × 20 ml). The combined organic layers were washed with a 1 M EDTA/NaOH solution (3 × 15 ml). After separation, the DCM fraction was dried over $MgSO_4$ and filtered by gravity filtration. The solvent was removed *in* vacuo, and the crude product was then column chromatographed on silica gel using DCM–MeOH (99:1) as the eluent. The solvent was removed *in vacuo* which afforded ligand **L3** as a dark-orange crystalline solid (0.85 g, 89%). FT-IR (ATR, ν): 1600 cm^{-1} (C=N). ^1H NMR (chloroform-d, 600 MHz): δ 8.60 (d, 1H, $^3J_{H-H}$ = 4.9 Hz, H^1); δ 8.28 (d, 1H, $^3J_{H-H}$ = 7.9 Hz, H^4); δ 8.23 (s, 1H, H^7); δ 7.82 (td, 1H, $^3J_{H-H}$ = 7.7 Hz, $^4J_{H-H}$ = 1.8 Hz, H^3); δ 7.33 (t, 1H, $^3J_{H-H}$ = 7.7 Hz, H^{11}); δ 7.25 (dd, 1H, $^3J_{H-H}$ = 4.8 Hz, $^4J_{H-H}$ = 1.2 Hz, H^2); δ 7.20 (d, 2H, $^3J_{H-H}$ = 7.7 Hz, H^{10}) δ 2.06 (s, 6H, Me). ^1H NMR (DMSO-d_6, 300 MHz): δ 8.80 (s, 1H, H^7); δ 8.63 (dq, 1H, $^3J_{H-H}$ = 4.8 Hz, $^4J_{H-H}$ = 1.0 Hz, H^1); δ 8.15 (dt, 1H, $^3J_{H-H}$ = 7.9 Hz, $^4J_{H-H}$ = 1.2 Hz, H^4); δ 7.95 (td, 1H, $^3J_{H-H}$ = 7.6 Hz, $^4J_{H-H}$ = 1.8 Hz, H^3); δ 7.45–7.36 (comp., 2H, $H^{2,11}$); δ 7.34–7.28 (comp., 2H, H^{10}); δ 1.99 (s, 6H, Me). $^{13}C\{1H\}$ NMR (chloroform-d, 151 MHz): δ 150.4 (C_{Ar}); δ 149.6 (C_{Ar}); δ 148.5 (C_{Ar}); δ 137.1 (C_{Ar}); δ 136.0 (C_{Ar}); δ 135.6 (C_{Ar}); δ 130.2 (C_{Ar}); δ 128.6 (C_{Ar}); δ 124.0 (C_{Ar}); δ 123.1 (C_{Ar}); δ 120.5 (C_{Ar}); δ 17.6 (C_{Me}). HRMS (ESI+ mode, m/z): calcd for $[M + H]^+$ 251.1297; found 251.1302. Anal. calcd. (%) for $C_{15}H_{14}N_4 \cdot 0.1CH_2Cl_2$: C, 70.39; H, 5.55; N, 21.77; found: C, 70.83; H, 5.48; N, 21.71.

4.3.2 | Synthesis of 1-octyl-4-pyridyl-*1H*-1,2,3-triazole ligated palladium methyl complex (C1)

To a stirred N_2-degassed solution of (COD)PdMeCl (0.26 g, 1.00 mmol) dissolved in DCM (3 ml) was added ligand **L1** (0.28 g, 1.1 mmol) dissolved in DCM (3 ml) and the reaction was stirred for 2 h at room temperature. After the allotted time, the solution was concentrated by reducing the solvent volume *in vacuo*. The DCM solution was layered with Et_2O, resulting in the product precipitating out of solution. The precipitate was filtered and washed with Et_2O which afforded the product as a light-yellow powder (0.36 g, 87%). FT-IR (ATR, υ): 1614 cm^{-1} (C=N). ^1H NMR (chloroform-d, 600 MHz): δ 8.68 (d, 1H, $^3J_{H-H}$ = 5.2 Hz, H^1); δ 8.37 (s, 1H, H^7); δ 7.80 (td, 1H, $^3J_{H-H}$ = 8.0 Hz, $^4J_{H-H}$ = 1.4 Hz, H^3); δ 7.73 (d, 1H, $^3J_{H-H}$ = 8.0 Hz, H^4); δ 7.27 (dd, 1H, $^3J_{H-H}$ = 5.3 Hz, $^4J_{H-H}$ = 1.1 Hz, H^2); δ 4.45 (t, 2H, $^3J_{H-H}$ = 7.6 Hz, H^8); δ 1.96 (quin., 2H, $^3J_{H-H}$ = 7.1 Hz, H^9); δ 1.39–1.19 (comp., 10H, H^{10-14}); δ 1.11 (s, 3H, H^{Pd-Me}); δ 0.86 (t, 3H, $^3J_{H-H}$ = 6.9 Hz, H^{15}). ^1H NMR (DMSO-d_6, 400 MHz): δ 9.17 (s, 1H, H^7); δ 8.72 (d, 1H, $^3J_{H-H}$ = 5.3 Hz, H^1); δ 8.16 (t, 1H, $^3J_{H-H}$ = 7.9 Hz, H^3); δ 8.06 (d, 1H, $^3J_{H-H}$ = 8.1 Hz, H^4); δ 7.64 (t, 1H, $^3J_{H-H}$ = 6.5 Hz, H^2); δ 4.52 (t, 2H, $^3J_{H-H}$ = 7.3 Hz, H^8); δ 1.95–1.84 (comp., 2H, H^9); δ 1.36–1.16 (comp., 10H, H^{10-14}); δ 0.98 (s, 3H, H^{Pd-Me}); δ 0.84 (t, 3H, $^3J_{H-H}$ = 6.8 Hz, H^{15}). $^{13}C\{^1H\}$ NMR (chloroform-d, 151 MHz): δ 148.3 (C^{Ar}); δ 148.2 (C^{Ar}); δ 146.6 (C^{Ar}); δ

138.2 (C^{Ar}); δ 124.7 (C^{Ar}); δ 123.7 (C^{Ar}); δ 123.4 (C^{Ar}); δ 120.9 (C^{Ar}); δ 52.6 ($C^{aliphatic}$); δ 31.8 ($C^{aliphatic}$); δ 30.0 ($C^{aliphatic}$); δ 29.1 ($C^{aliphatic}$); δ 29.0 ($C^{aliphatic}$); δ 26.5 ($C^{aliphatic}$); δ 22.7 ($C^{aliphatic}$); δ 14.2 ($C^{aliphatic}$); δ −6.9 ($C^{Pd–Me}$). HRMS (ESI+ mode, *m*/*z*): calcd for $[M - Cl + MeCN]^+$ 420.1980, found 420.1394. Anal. calcd (%) for $C_{16}H_{25}ClN_4Pd$: C, 46.28; H, 6.07; N, 13.49; found: C, 46.04; H, 6.18; N, 13.57.

4.3.3 | Synthesis of [Pd(Me)(CH_3CN)(L5)][PF_6] (C9)

To a stirred N_2-degassed suspension of complex **C5** (130 mg, 0.29 mmol) in MeCN (3 ml) was added $AgPF_6$ (88 mg, 0.349 mmol) dissolved in MeCN (3 ml) and the resulting solution was stirred for 3 h at room temperature. After the allotted time, the reaction was filtered over Celite and concentrated to the minimal volume under vacuum. Upon addition of Et_2O, the product precipitated out of solution as a white powder (153 mg, 88%). FT-IR (ATR, *υ*): 1618 cm^{-1} (C=N). ^1H NMR (acetonitrile-d_3, 600 MHz): δ 9.32 (s, 1H, H^7); δ 8.73 (d, 1H, $^3J_{H–H}$ = 5.2 Hz, H^1); δ 8.34 (td, 1H, $^3J_{H–H}$ = 7.8 Hz, $^4J_{H–H}$ = 1.6 Hz, H^3); δ 8.22 (d, 2H, $^3J_{H–H}$ = 8.5 Hz, $H^{9,10}$); δ 8.18 (d, 1H, $^3J_{H–H}$ = 8.1 Hz, H^4); δ 8.15 (d, 2H, $^3J_{H–H}$ = 8.5 Hz, $H^{9,10}$); δ 7.84–7.78 (m, 1H, H^2); δ 2.32 (s, 3H, $H^{Pd–Me}$); δ 1.53 (br, 3H, H^{MeCN}). $^{13}C\{^1H\}$ NMR (acetonitrile-d_3, 151 MHz): δ 151.1 (C^{Ar}); 150.2 (C^{Ar}); 146.9 (C^{Ar}); 141.8 (C^{Ar}); 139.7 (C^{Ar}); 132.7 (C^{Ar}); 128.6 (C^{Ar}); 127.5 (C^{Ar}); 125.6 (C^{Ar}); 124.2 (C^{Ar}); 123.8 (C^{Ar}); 122.9 (C^{Ar}); 122.6 (C^7), 1.8 (C^{MeCN}), −2.9 ($C^{Pd–Me}$). HRMS (ESI+ mode, *m*/*z*): calcd for $[M]^+$ 452.0314, found 452.0325; calcd for $[M - MeCN]^+$ 411.0049, found 411.0064. HRMS (ESI− mode, *m*/*z*): calcd for $[M]^-$ 144.9642, found 144.9635.

4.4 | X-ray crystal structure determination

Single X-ray diffraction intensity data were collected on a Bruker Apex DUO diffractometer with a CCD area detector[35] using graphite monochromated Mo-K*α* radiation (*λ* = 0.71073 Å). Data collection, reduction and refinement were performed using SMART and SAINT software.[36] Absorption corrections[37] and other systematic errors were accounted for using SADABS.[38] All structures were solved by Direct Methods and refined by full-matrix least-squares on F^2 using SHELXS-13 and SHELXL-16[39,40] within the X-Seed graphical user interface.[41,42] All non-hydrogen atoms were refined anisotropically, and hydrogen atoms were placed using calculated positions and riding models. High-resolution molecular diagrams were produced using the program POV-Ray.[43] CSD 1921497 for complex **C1**, CSD 1921498 for complex **C4**, CSD 1921499 for complex **C5**, CSD 1921500 for complex **C7** and CSD 1969487 for complex **C11** contain the supplementary crystallographic data for this paper.

4.5 | Procedure for preparative ethylene oligomerization

A 250 ml Parr stainless-steel high-pressure autoclave was charged with the required amount of toluene and co-catalyst and sealed under an inert atmosphere in a glovebox. The reactor was first brought to the set temperature at which point a dispersion of the pre-catalyst in toluene (total reaction volume: 40 ml) was added via syringe under positive ethylene pressure. The reactor was then pressurized with ethylene to the required pressure after which stirring commenced (150 rpm). The ethylene feed was maintained throughout the catalytic reaction, and the volume of ethylene consumed was monitored with a mass flow meter. After the allotted time, the reactor was cooled to −78°C; then the reactor was slowly vented to release excess ethylene. The reaction mixture was quenched with ethanol (5 ml) while maintaining the temperature below −20°C to minimize the loss of any volatile products. A liquid sample was filtered through a syringe filter and the filtrate analyzed by GC-FID using *p*-xylene as internal standard. No long-chain oligomers or polymers were produced during these reactions. Turnover frequencies were calculated from the volume of ethylene consumed during the reaction as a function of time.

ACKNOWLEDGEMENTS

The authors acknowledge the financial support by the National Research Foundation of South Africa (grant no. CPRR160408161799) and the c*change Centre of Excellence in Catalysis, the Department of Science and Technology, South Africa. The Division of Research Development at Stellenbosch University is also thanked for their financial support.

CONFLICT OF INTEREST

There are no conflicts to declare.

ORCID

Mohammed Cassiem Joseph https://orcid.org/0000-0003-1732-5592

Andrew John Swarts https://orcid.org/0000-0002-7942-8557

Selwyn Frank Mapolie https://orcid.org/0000-0001-6891-0412

REFERENCE

[1] C. Bianchini, G. Giambastiani, L. Luconi, A. Meli, *Coord. Chem. Rev.* **2010**, *254*, 431.
[2] D. H. Camacho, Z. Guan, *Chem. Commun.* **2010**, *46*, 7879.
[3] J. Skupinska, *Chem. Rev.* **1991**, *91*, 613.
[4] L. K. Johnson, C. M. Killian, M. Brookhart, *J. Am. Chem. Soc.* **1995**, *117*, 6414.
[5] C. M. Killian, L. K. Johnson, M. Brookhart, *Organometallics* **1997**, *16*, 2005.
[6] S. Svejda, M. Brookhart, *Organometallics* **1999**, *18*, 65.
[7] P. Kuhn, D. Sémeril, D. Matt, M. J. Chetcuti, P. Lutz, *Dalton Trans.* **2007**, 515.
[8] F. Speiser, P. Braunstein, L. Saussine, *Acc Chem. Res.* **2005**, *38*, 784.
[9] G. S. Nyamato, S. O. Ojwach, M. P. Akerman, *Organometallics* **2015**, *34*, 5647.
[10] A. Baschieri, S. Muzzioli, V. Fiorini, E. Matteucci, M. Massi, L. Sambri, S. Stagni, *Organometallics* **2014**, *33*, 6154.
[11] L. Bernet, R. Lalrempuia, W. Ghattas, H. Mueller-bunz, L. Vigara, A. Llobet, M. Albrecht, *Chem. Commun.* **2011**, *47*, 8058.
[12] A. Bolje, D. Urankar, J. Košmrlj, *Eur. J. Org. Chem.* **2014**, *2014*, 8167.
[13] J. D. Crowley, P. H. Bandeen, L. R. Hanton, *Polyhedron* **2010**, *29*, 70.
[14] A. J. Swarts, S. F. Mapolie, *Dalton Trans* **2014**, *43*, 9892.
[15] M. C. Joseph, A. J. Swarts, S. F. Mapolie, *Dalton Trans.* **2018**, *47*, 12209.
[16] A. J. Swarts, F. Zheng, V. J. Smith, E. Nordlander, S. F. Mapolie, *Organometallics* **2014**, *33*, 2247.
[17] R. E. Rulke, J. M. Ernsting, A. L. Spek, C. J. Elsevier, P. W. N. M. van Leeuwen, K. Vrieze, *Inorg. Chem* **1993**, *32*, 5769.
[18] X. L. Chen, J. Gao, H. Liao, H. Y. Gao, Q. Wu, *Chin. J. Polym. Sci. (Engl. Edn)* **2018**, *36*, 176.
[19] L. Guo, W. Liu, K. Li, M. Sun, W. Sun, L. Zhao, G. Jiang, H. Peng, Z. Liu, S. Dai, *Eur. Polym. J.* **2019**, *115*, 185.
[20] A. Bastero, C. Claver, A. Ruiz, S. Castillûn, E. Daura, C. Bo, E. Zangrando, *Chem. A Eur. J.* **2004**, *10*, 3747.
[21] H. Wu, Y. Liu, S. Peng, S. Liu, *Eur. J. Inorg. Chem.* **2003**, *2003*, 3152.
[22] M. D. Doherty, S. Trudeau, P. S. White, J. P. Morken, M. Brookhart, *Organometallics* **2007**, *26*, 1261.
[23] M. Navarro, V. Rosar, T. Montini, B. Milani, M. Albrecht, *Organometallics* **2018**, *37*, 3619.
[24] V. Khlebnikov, A. Meduri, H. Mueller-Bunz, T. Montini, P. Fornasiero, E. Zangrando, B. Milani, M. Albrecht, *Organometallics* **2012**, *31*, 976.
[25] C. T. Burns, R. F. Jordan, *Organometallics* **2007**, *26*, 6726.
[26] C. T. Burns, R. F. Jordan, *Oraganometallics* **2007**, *26*, 6737.
[27] M. M. Mogorosi, T. Mahamo, J. R. Moss, S. F. Mapolie, J. C. Slootweg, K. Lammertsma, G. S. Smith, *J. Organomet. Chem.* **2011**, *696*, 3585.
[28] S. Adewuyi, G. Li, S. Zhang, W. Wang, P. Hao, W.-H. Sun, N. Tang, J. Yi, *J Organomet. Chem.* **2007**, *692*, 3532.
[29] X. Tang, W. H. Sun, T. Gao, J. Hou, J. Chen, W. Chen, *J. Organomet. Chem* **2005**, *690*, 1570.
[30] W. Oberhauser, G. Manca, A. Ienco, C. Strabler, J. Prock, A. Weninger, R. Gutmann, P. Bruggeller, *Organometallics* **2014**, *33*, 4067.
[31] D. Drew, J. R. Doyle, A. G. Shaver, *Inorg. Synth.* **1990**, *28*, 346.
[32] M. H. Ngai, P.-Y. Yang, K. Liu, Y. Shen, M. R. Wenk, S. Q. Yao, M. J. Lear, *Chem. Commun* **2010**, *46*, 8335.
[33] Z. Dai, Y. Chen, M. Zhang, S. Li, T. Yang, L. Shen, J. Wang, S. Qian, H. Zhu, Y. Ye, *Org. Biomol. Chem* **2015**, *13*, 477.
[34] N. Moitra, J. Moreau, X. Cattoen, M. Man, *Chem. Commun* **2010**, *46*, 8416.
[35] Apex2, *Data Collect Software*Bruker AXS **2010**.
[36] SAINT, *Data Reduct*, Software, Bruker AXS **2003**.
[37] R. H. Blessing, *Acta Crystallogr. A* **1995**, *51*, 33.
[38] SADABS, *Version 205,* Bruker AXS, **2002**.
[39] G. M. Sheldrick, *Acta Crystallogr., Sect A: Found. Crystallogr.* **2007**, *64*, 112.
[40] G. M. Sheldrick, *Acta Crystallogr. Sect. C* **2015**, *74*, 3.
[41] J. L. Atwood, L. J. Barbour, *Cryst. Growth Des.* **2003**, *3*, 3.
[42] L. J. Barbour, *J Supramol Chem* **2001**, *1*, 189.
[43] POV-Ray, *Version 36*, Williamstown, Australia, Persistence of vision ray.

SUPPORTING INFORMATION

Additional supporting information may be found online in the Supporting Information section at the end of this article.

How to cite this article: Joseph MC, Swarts AJ, Mapolie SF. Palladium (II) complexes chelated by 1-substituted-4-pyridyl-*1H*-1,2,3-triazole ligands as catalyst precursors for selective ethylene dimerization. *Appl Organometal Chem*. 2020;e5595. https://doi.org/10.1002/aoc.5595